

Chemical trend of exchange couplings in diluted magnetic II-VI semiconductors

T. Chanier,¹ F. Viot,¹ and R. Hayn¹

¹*Institut de Matériaux, Microélectronique et Nanosciences de Provence,
Faculté St. Jérôme, Case 142, F-13397 Marseille Cedex 20, France*

(Dated: May 13, 2018)

Abstract

We have calculated the chemical trend of magnetic exchange parameters (J_{dd} , $N\alpha$, and $N\beta$) of Zn-based II-VI semiconductors ZnA (A=O, S, Se, and Te) doped with Co or Mn. We show that a proper treatment of electron correlations by the LSDA+ U method leads to good agreement between experimental and theoretical values of the nearest-neighbor exchange coupling J_{dd} between localized $3d$ spins in contrast to the LSDA method. The exchange couplings between localized spins and doped electrons in the conduction band $N\alpha$ are in good agreement with experiment as well. But the values for $N\beta$ (coupling to doped holes in the valence band) indicate a cross-over from weak coupling (for A=Te and Se) to strong coupling (for A=O) and a localized hole state in ZnO:Mn. That hole localization explains the apparent discrepancy between photoemission and magneto-optical data for ZnO:Mn.

PACS numbers: 75.50.Pp,71.23.An,71.55.Gs

I. INTRODUCTION

After the seminal discovery of ferromagnetism in GaAs:Mn¹ with a critical temperature T_c as high as 110 K there is worldwide a renewed interest in diluted magnetic semiconductors (DMS). Recently, the Curie temperature in GaAs:Mn could be pushed to values of about 180 K by a careful control of the annealing conditions during the growth process.² There is a great search activity to look for alternative materials, especially in the class of II-VI semiconductors (SC). Ferromagnetism (FM) in diluted II-VI SC is known for a long time with up to now low T_c values, however.³ They also serve as model materials since they allow to control the magnetic ions and the doped charge carriers independently. In such a way it was possible to demonstrate the carrier-induced mechanism of the ferromagnetic state in Pb-doped SnTe:Mn⁴ or in p -doped ZnTe:Mn.⁵

The DMS combine ferromagnetism with the conductivity properties of semiconductors. Therefore, they are ideal materials for applications in spintronics where not only the electron charge but also the spin of the charge carrier is used for information processing. For instance, they allow to resolve the conductivity mismatch problem which hinders a high polarizability of injected electrons in a ferromagnetic metal/semiconductor junction.⁶

The ferromagnetism in the traditionally known DMS arises due to Zener's p - d exchange mechanism.⁷ The $3d$ transition metal impurities lead to localized spins \mathbf{S}_i . Hole doping into the valence band (either by the $3d$ transition metals itself or by other acceptor impurities) provides charge carriers whose spins interact with the $3d$ spins. This local p - d exchange coupling $J_{pd}^v = N\beta$ leads to a parallel arrangements of the magnetic moments since a ferromagnetic state allows a higher mobility of the doped holes. For a high doping level the material becomes more metallic and the mechanism changes to a RKKY-like interaction.

From this argumentation follows immediately that the crucial parameter to increase T_c is the J_{pd}^v coupling. Indeed, a simple theory of Zener's p - d exchange mechanism⁸ gives $T_c \propto (J_{pd}^v)^2 x_h$ where x_h is the hole doping level. It can be expected from general grounds that a decreasing anion-cation distance leads to an increase of the p - d tight-binding hopping parameter t_{pd} , and consequently to an increase of J_{pd}^v . That reasoning lead Dietl *et al*⁸ to the proposal of room temperature ferromagnetism in Mn-doped ZnO or GaN, respectively, which created a tremendous activity and numerous reports on room temperature FM in II-VI DMS or similar materials.^{9,10,11}

However, there are serious doubts whether the reported room temperature ferromagnetism belongs really to the same class of ferromagnetism as that one observed in GaAs:Mn or ZnTe:Mn which is based on Zener's p - d exchange mechanism. For instance, in ZnO:Co ferromagnetism was reported in samples produced by laser ablation,^{10,11} or by the sol-gel method,⁹ whereas other samples fabricated by precursor deposition,¹² or molecular beam epitaxy (MBE)^{13,14} showed no signs of ferromagnetism and antiferromagnetic couplings between nearest neighbor $3d$ spins. It is highly probable that the observed ferromagnetic effects in ZnO:Co are due to uncompensated spins at the surface of Co-rich antiferromagnetic nanoclusters.¹⁵

The proposal of Dietl *et al*⁸ was based on simple model calculations and qualitative arguments. There is a real need for a parameter free *ab-initio* study of the relevant exchange parameters in II-VI semiconductors to put the expected chemical tendency on a firm basis. Such a calculation of the nearest neighbor couplings of local spins J_{dd} and the p - d exchange couplings J_{pd}^v and J_{pd}^c with valence and conduction bands, respectively, is presented here. We considered the series of Co- and Mn-doped ZnA with the anions A=Te, Se, S and O.

To achieve our goal we had to solve two theoretical problems. First of all, the local spin density approximation (LSDA) is not sufficient. It leads to wrong predictions of FM in ZnO:Co even without additional hole doping,¹⁶ to too large values of $|J_{dd}|$ for ZnO:Mn, and to the wrong (FM) sign of one of the two nearest neighbor exchange couplings in wurtzite ZnO:Co.¹⁷ It was shown that this deficiency of LSDA can be repaired by taking into account the strong Coulomb correlation in the $3d$ shell by the LSDA+ U method. To choose the U values we have to take into account that they decrease in the series from O to Te due to an increase of screening effects. The values of J_{dd} are very well known experimentally in this series. Therefore they can be used to check the chosen U values. We will show below that for reasonable values of U we obtain J_{dd} in good agreement with experimental results and we may explain the chemical tendency.

The second theoretical problem concerns the p - d exchange coupling between the localized spins and the holes in the valence band J_{pd}^v . This coupling leads to the giant Zeemann effect¹⁸ and it is seen in our calculations by a band-offset ΔE^v between spin up and spin down of the valence band. For small values of J_{pd}^v (which means also small values of t_{pd}) both splittings, the experimental and the theoretical one, are proportional to the magnetic impurity concentration x . In that weak coupling regime the p - d coupling can be simply

calculated by using the proportionality between splitting and x . We will show, however, that there are more and more deviations from $\Delta E^v \propto x$ if we go from ZnTe to ZnO. The exchange values obtained in that manner seem to depend on the concentration of magnetic impurities. We solve that problem by a fit to the Wigner-Seitz approach of Benoit and Guillaume *et al.*¹⁹ Our results prove that we reach the strong coupling limit for ZnO. As we will show below, in that case the impurity potential is so strong that it can bind a hole for ZnO:Mn, whereas ZnO:Co is close to the localized limit.

Our ab-initio results strengthen the recent model calculations in Ref. 20. That work was aimed to explain the tremendous difference between the experimental J_{pd}^v values obtained from photoemission and magneto-optics, especially in ZnO and GaN.²¹ It was argued that this difference arises due to state localization which is confirmed by our ab-initio calculations below. But we also will show that our results for $|N\beta|$ are much smaller than those evaluated earlier from photoemission for ZnO:Mn (-2.7 eV (Ref. 22) or -3.0 eV (Ref. 23)) and ZnO:Co (-3.4 eV (Ref. 24)) and which were used as model input parameters in Ref. 20.

The organization of our paper is as follows. After presenting the super-cell method in Sec. II, we discuss the nearest neighbor exchange coupling in Sec. III. That fixes the U values unambiguously. In Sec. IV we present our results for $J_{pd}^v = N\beta$ and $J_{pd}^c = N\alpha$. Finally, in Sec. V we discuss the arguments in favor of a localized state in ZnO:Mn.

II. SUPER-CELL CALCULATIONS

We used super-cell calculations to determine the exchange couplings J_{dd} , $N\alpha$, and $N\beta$. Since we are mainly interested in the chemical tendency within the II-VI series we restrict our study to the zinc-blende structure. All compounds of the series exist in that modification, even ZnO as epitaxial layer. To calculate J_{dd} we used super-cells of the form $T_2Zn_6A_8$ with the transition metals $T=Co$ or Mn and with the anions $A=O, S, Se,$ and Te . In those super-cells the magnetic ions build chains. The exchange constants are then determined by comparing the total energies of ferro- and antiferromagnetic arrangements. We have checked that the influence of finite size effects is negligible (not larger than 6 per cent for J_{dd}) by performing some calculations with $T_2Zn_{14}A_{16}$ super-cells.

For J_{pd}^v we used super-cells with three different concentrations of magnetic ions, $x = 1/4$, $x = 1/8$, and $x = 1/32$, i.e. TZn_3A_4 , TZn_7A_8 and $TZn_{31}A_{32}$. As will be explained below,

these numerical results have to be fitted with the Wigner-Seitz approach to obtain J_{pd}^v . In all calculations we used the experimental lattice constants $a = 6.101 \text{ \AA}$, 5.668 \AA , and 5.410 \AA for ZnTe, ZnSe, and ZnS, respectively.^{25,26} For ZnO we used a lattice constant $a = 4.557 \text{ \AA}$ which gives the same unit cell volume as the experimental value. (Bulk ZnO has $a = 3.2427 \text{ \AA}$ and $c = 5.1948 \text{ \AA}$ in the wurtzite structure.)²⁷

The super-cell calculations were performed using the full-potential local-orbital (FPLO) band structure scheme.²⁸ In the FPLO method (version FPLO5) a minimum basis approach with optimized local orbitals is employed, which allows for accurate and efficient total energy calculations. For the present calculations we used the following basis set: Zn,Co,Mn: $3s3p:4s4p3d$, O: $2s2p;3d$, S: $3s3p3d$, Se: $4s4p3d$, and Te: $5s5p4d$. The site-centered potentials and densities were expanded in spherical harmonic contributions up to $l_{max} = 12$.

The exchange and correlation potential was treated in two different ways. First, the local spin-density approximation (LSDA) was used in the parametrization of Perdew and Wang.²⁹ However, as will be shown below in more detail, this approximation has severe deficiencies in the present case. The energetical positions of the Co(Mn) $3d$ states with respect to the valence band are incorrectly given in the LSDA calculation. They are expected to be much lower in energy and this correlation effect was taken into account by using the FPLO implementation of the LSDA+ U method in the atomic limit scheme.^{30,31} The convergence of the total energies with respect to the \mathbf{k} -space integrations were checked for each of the super-cells independently. The calculations for each cell were first performed within the LSDA approximation using basis optimization. The LSDA+ U calculations were then made starting from the LSDA optimized basis but with no basis optimization in the self-consistency cycle in order to obtain convergence. The Slater parameters F^2 and F^4 for Mn and Co in the LSDA+ U calculations were chosen close to atomic values, namely $F^2 = 7.4 \text{ eV}$ and $F^4 = 4.6 \text{ eV}$ (corresponding to the Hund exchange coupling $J_H = 0.86 \text{ eV}$) for Mn, and $F^2 = 7.9 \text{ eV}$ and $F^4 = 5.0 \text{ eV}$ ($J_H = 0.92 \text{ eV}$) for Co. The Slater parameter $F^0 = U$, however, is much more screened and its influence has been investigated more in detail (see below).

III. D-D EXCHANGE COUPLINGS

In this Section we are going to determine the exchange couplings between two localized magnetic ions. We are considering two nearest neighbor impurities, each carrying a local

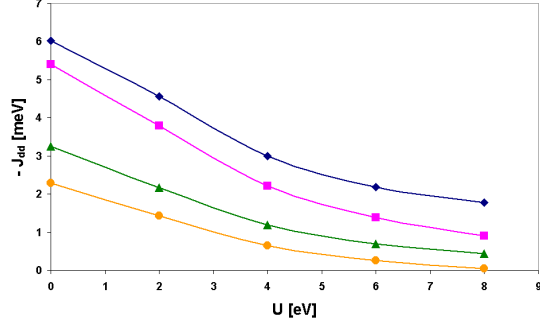


FIG. 1: (Color online) Calculated exchange couplings J_{dd} for ZnA:Mn (from above to below: A=0 (blue), S (red), Se (green), and Te (yellow)) as a function of the Coulomb correlation U in the $3d$ shell.

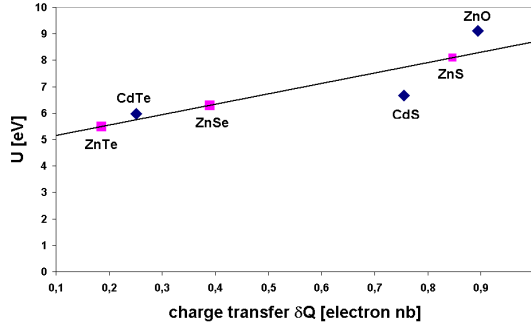


FIG. 2: (Color online) Coulomb correlation U in the $3d$ shell of Mn-impurities in II-VI-SC as function of charge transfer δQ . The values for CdTe, CdS, and ZnO are taken from Ref. 32 (constrained DFT-calculations, blue diamonds) and the other values (red squares) by linear interpolation corresponding to the calculated charge transfer.

spin \mathbf{S}_i . Then, the Heisenberg Hamiltonian for a localized pair of spins is given by

$$H = -2J_{dd}\mathbf{S}_i\mathbf{S}_j . \quad (1)$$

The corresponding total energies per magnetic ion for ferromagnetic (FM) and antiferromagnetic (AFM) arrangements of the two spins, E_{FM} and E_{AFM} , lead to the energy difference between the FM and AFM states:

$$\Delta E = \frac{E_{FM} - E_{AFM}}{2} = -\frac{J_{dd}}{2}S_T(S_T + 1) , \quad (2)$$

TABLE I: Comparison of calculated and experimental values for the nearest neighbor exchange couplings J_{dd} for ZnA:Mn.

	exp.	LSDA+ U		LSDA
	J_{dd}^{exp} (meV)	J_{dd} (meV)	U (eV)	J_{dd} (meV)
ZnO:Mn	-2.09 ^a	-2.18	6	-6.02
ZnS:Mn	-1.41 ^b ; -1.39 ^c	-1.39	6	-5.41
ZnSe:Mn	-1.05 ^d ; -1.06 ^c	-1.19	4	-3.25
ZnTe:Mn	-0.75 ^e ; -0.76 ^f	-0.65	4	-2.29

^aMagnetization step method, Ref. 33, first neighbor in the (a,b) plane of the wurtzite structure.

^bMagnetization step method, Ref. 34.

^cInelastic neutron scattering, Ref. 35.

^dMagnetization step method, Ref. 36.

^eMagnetization step method, Ref. 37.

^fInelastic neutron scattering, Ref. 38.

TABLE II: Comparison of calculated and experimental values for the nearest neighbor exchange couplings J_{dd} for ZnA:Co.

	exp.	LSDA+ U		LSDA
	J_{dd}^{exp} (meV)	J_{dd} (meV)	U (eV)	J_{dd} (meV)
ZnO:Co	-2.0 ^a	-1.73	6	-1.39
ZnS:Co	-4.09 ^b	-4.13	4	-7.26
ZnSe:Co	-4.26 ^c	-3.36	4	-6.26
ZnTe:Co	-3.27 ^c	-3.32	4	-6.94

^aInelastic neutron scattering, Ref. 39, first neighbor in the (a,b) plane of the wurtzite structure.

^bInelastic neutron scattering, Ref. 40.

^cInelastic neutron scattering, Ref. 41.

where S_T is the total spin of two parallel spins S , i.e. $S_T = 3$ or 5 for Co or Mn. That energy difference can be compared with the corresponding energy differences of isolated pairs in the large super-cells. Those super-cells where the magnetic ions form chains are different, however. Then, each magnetic ion has two nearest neighbor magnetic ions which doubles approximatively the previous energy difference (2). The exact energy difference between FM

and AFM states of a Heisenberg chain is slightly different, but that is unimportant for our present argumentation.

The calculated exchange constants J_{dd} show a strong variation with U . That is illustrated in Fig. 1 for the Mn-doped compounds. In that case the tendency is monotonous, i.e. the increase of U leads to a decrease of J_{dd} . A similar tendency is visible for ZnA:Co with the exception of ZnO:Co where the LSDA exchange constant is only -1.39 meV and not of the order of -6...-7 meV like for the other compounds. This exception is due to ferromagnetic contributions in ZnO:Co as analyzed in Ref. 17.

The experimental values of J_{dd} are known with great accuracy by magnetization step measurements or inelastic neutron scattering (see Tables I, II). The comparison of experimental and theoretical values shows that the LSDA method strongly overestimates the exchange couplings. In our method the Hubbard correlation has to be chosen between 4 and 6 eV to obtain the correct exchange couplings. The precise value of U has also a chemical tendency. That was revealed in Ref. 32 and can be explained since the compounds ZnA become less and less ionic in going from A=Zn to A=Te. The decrease of ionicity can be measured by a decrease of the charge transfer towards the magnetic ion in the series (Fig. 2). The charge transfer is correlated with the calculated U value in the constrained density functional calculation.³² Taking into account this chemical tendency we chose the U values of Tables I, II to calculate J_{dd} (and $N\alpha$, $N\beta$ in the next Chapter). Those values for U are slightly smaller than that one calculated in Ref. 32 since the FPLO and LMTO (linearized muffin tin orbitals) implementations of the LSDA+ U method are not equivalent. Taking into account the restricted accuracy of our procedure we varied U in steps of 2eV. Then we obtain the theoretical results of Tables I, II which are in good agreement with the experimental values.

IV. P-D EXCHANGE COUPLINGS

The localized magnetic moments \mathbf{S}_i which are provided by the magnetic ions Co^{2+} or Mn^{2+} interact with the spin of doped holes \mathbf{s} . This interaction can be parametrized in the continuum approximation in the form:

$$\hat{H} = -\beta \sum_i \mathbf{S}_i \mathbf{s} \delta(\mathbf{r} - \mathbf{R}_i) , \quad (3)$$

where the magnetic impurities are placed at \mathbf{R}_i . A similar interaction exists with the spin of doped electrons which is usually denoted by the parameter α . If we transform the Hamiltonian into a lattice model, the interaction (3) becomes

$$\hat{H} = -J_{pd}^v \sum_i \mathbf{S}_i \mathbf{s}_i, \quad (4)$$

with the sum over all lattice sites i which are occupied by magnetic impurities, and where \mathbf{s}_i is the local spin operator of the doped hole in the lattice representation. Both parameters are connected by $J_{pd}^v = N\beta$ where N is the number of cations per volume ($N = 4/a^3$ in the zinc blende structure). One possibility to measure $N\beta$ is photoemission where the hole in the valence band is created during the photoemission process. Another possibility is magneto-optics which measures the giant Zeeman effect of excitons, i.e. electron-hole pairs.

We calculated the p - d exchange coupling with super-cells having impurity concentrations of $x = 1/4$, $1/8$, and $1/32$ magnetic ions. The p - d exchange coupling leads to a valence band and conduction band offset between spin up and spin down ΔE^v and ΔE^c . In the case of weak p - d coupling, this band offset is proportional to the impurity concentration x , i.e. it can be calculated in mean-field theory. That can be clearly observed in our numerical data and the corresponding exchange couplings are then simply given by

$$J_{pd}^c = N\alpha = \frac{\Delta E^c}{x\langle S \rangle} \text{ and } J_{pd}^v = N\beta = \frac{\Delta E^v}{x\langle S \rangle}, \quad (5)$$

where $\langle S \rangle = \langle M \rangle / (2\mu_B)$ is the mean value of the local spin calculated within the ab-initio approach. For the Mn compounds, the calculated magnetization values are very close to saturation ($\langle M \rangle / \mu_B = 5.00, 4.85, 4.83$, and 4.85 in the series with the anions A=O, S, Se, and Te, respectively) but there are stronger deviations from the local value $S = 3/2$ for the Co ones ($\langle M \rangle / \mu_B = 3.00, 2.65, 2.75$, and 2.61 in the same series).

The mean-field approach works very well for $N\alpha$ which has small values in all cases. The reason is the small coupling between the conduction band, which is built by Zn $4s$ - $4p$ hybridized states, with the impurity states. The calculated values are also in excellent agreement with the available experimental data (see Tables III and IV).

The situation is different for $N\beta$. The valence band is built by the anion p -orbitals which have generally a large overlap with impurity states. Therefore, $N\beta$ is much more important than $N\alpha$. And this tendency is increased when the lattice constant diminishes in going from Te to O. As a consequence, the mean-field description, and the proportionality between band-

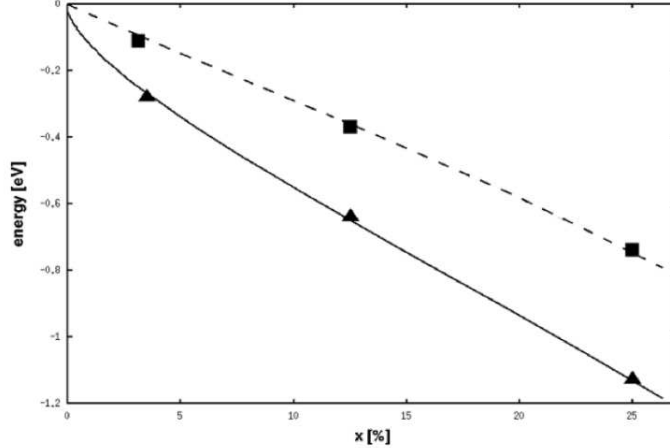


FIG. 3: Valence band-edge spin splitting ΔE^v of ZnO:Mn (triangles) and ZnTe:Mn (squares) calculated with the LSDA+ U method. The solid (dashed) lines represent the fit to the Wigner-Seitz model.

offset and impurity concentration breaks down. Historically, the deviation from the mean-field picture was first observed experimentally for CdS:Mn.⁴² In our calculations, deviations from the mean-field behavior are especially visible for doped ZnO and ZnS. They are mostly pronounced for ZnO:Mn (see Fig. 3) where a localized state appears which means that ΔE^v tends to a constant value for $x \rightarrow 0$ (see next Section). Formally, the mean-field calculation of $N\beta$ (5) leads then to a divergent value which illustrates the discussed break-down in the most prominent way. This can also be interpreted as a crossover from the weak coupling to the strong coupling regime in the series going from Te to O. Since the localization is expected to disappear for higher impurity concentrations (visible in a band merging of the localized state with the valence band in the density of states) there is some justification to use the mean-field formula (5) for $x = 1/4$. The values of $N\beta^{MF}$ calculated in that way are displayed in Tables III and IV.

To resolve the deviations from the mean-field behavior a Wigner-Seitz approach was developed.¹⁹ We will use it to calculate $N\beta$ more accurately (see also Ref. 43 for GaAs:Mn). In that theory, the valence band is described in the effective mass approximation with a spin dependent impurity potential. The Hamiltonian for one impurity has the form:

$$\hat{H} = -\frac{\hbar^2}{2m^*} \frac{\partial^2}{\partial \mathbf{r}^2} + (W - J_{pd}^v \mathbf{S}_i \mathbf{s}) \Theta(b - r). \quad (6)$$

Replacing the spin operator \mathbf{s} by s_z we obtain a spin polarized scattering potential

$$\hat{H}_\sigma = -\frac{\hbar^2}{2m^*} \frac{\partial^2}{\partial \mathbf{r}^2} + U_\sigma \Theta(b - r) , \quad (7)$$

where $\sigma = +1(-1) = \uparrow (\downarrow)$ and $U_\sigma = W - \sigma S J_{pd}^v/2$ with the local spin $S = 5/2$ and $3/2$ for Mn and Co, respectively. The muffin-tin radius of the scattering potential b was fixed such that the corresponding spheres around the cations fill in completely the space of the solid, i.e. $(4\pi/3)b^3 = a^3/4$. The finite concentration of impurities is taken into account by the condition that the derivative of the wave function $\Psi'(R) = 0$ vanishes at the mean radius R around each impurity which is determined by $(4\pi/3)R^3 = 1/(Nx)$. The scattering problem for each spin direction is easy to solve¹⁹ and the lowest eigenvalue for spin up (down) E_\uparrow (E_\downarrow) is given by a transcendental equation. The valence band splitting can be expressed as

$$\Delta E^v = E_\downarrow - E_\uparrow = \frac{4\pi b^3}{3} Nx [U_\downarrow \delta(x, \eta_\downarrow) - U_\uparrow \delta(x, \eta_\uparrow)] , \quad (8)$$

where $\delta(x, \eta_\sigma) = |E_\sigma/E_\sigma^{MF}|$ is the ratio of this eigenvalue to the mean-field result

$$E_\sigma^{MF} = \frac{4}{3} \pi b^3 U_\sigma Nx . \quad (9)$$

The deviation is controlled by the dimensionless fitting parameter

$$\eta_\sigma = \frac{U_\sigma}{|U_c|} = 2m^* U_\sigma \left(\frac{2b}{\pi \hbar} \right)^2 , \quad (10)$$

where U_c is the critical potential value for the bound state creation.

For the fit we used the gap and the band-offset calculated within the LSDA+ U approach for the three concentrations mentioned above. We used the experimental values for the effective masses $m^*/m = 0.22, 0.21, 0.32$, and 1.0 for ZnA, A=Te, Se, S, and O, respectively. These values were obtained by averaging over the transversal (light) and longitudinal (heavy) effective masses according to $3/m^* = 2/m_t + 1/m_l$.¹⁹ In Fig. 3 we compare the weak coupling case (represented by ZnTe:Mn) having a linear dependence of the band-offset on the impurity concentration x with the strong coupling compound ZnO:Mn showing clear deviations from linearity. The Wigner-Seitz approach fits well our numerical data and leads to a localized state for ZnO:Mn. A summary of all the results is presented in Tables III and IV.

V. LOCALIZED STATE

The Wigner-Seitz fit for ZnO:Mn results in the dimensionless coupling parameter $\eta_\downarrow = -1.12$ corresponding to a localized hole state. That is also directly visible in the density of

TABLE III: Comparison of experimental and theoretical values of the p - d exchange couplings with the conduction ($N\alpha$) and valence ($N\beta$) bands for ZnA:Mn (A=O, S, Se, and Te). The theoretical results were obtained by the LSDA+ U method, analyzed within the mean-field approximation ($N\alpha^{MF}$ and $N\beta^{MF}$) and the Wigner-Seitz approach¹⁹ ($N\beta^{WS}$). Also given are the dimensionless coupling parameters η_{\uparrow} and η_{\downarrow} of the Wigner-Seitz approach.

	$N\alpha^{exp}$ (eV)	$N\beta^{exp}$ (eV)	$N\alpha^{MF}$ (eV)	$N\beta^{MF}$ (eV)	$N\beta^{WS}$ (eV)	η_{\uparrow}	η_{\downarrow}
ZnO:Mn	—	0.1 ^a ; -2.7 ^b ; -3.0 ^c	0.38	-1.81	-1.42	0.08	-1.12
ZnS:Mn	—	-1.3 ^b	0.11	-1.39	-1.12	0.07	-0.36
ZnSe:Mn	0.26 ^d	-1.31 ^d ; -1.0 ^b	0.29	-1.46	-1.23	0.05	-0.29
ZnTe:Mn	0.18 ^e	-1.05 ^e ; -0.9 ^b	0.23	-1.22	-1.02	0.04	-0.29

^aMagneto optical measurements, Ref. 44.

^bPhotoemission spectroscopy, Ref. 22.

^cPhotoemission spectroscopy, Ref. 23.

^dMagneto optical measurements, Ref. 45.

^eMagneto optical measurements, Ref. 46.

TABLE IV: The same as Table III but for ZnA:Co.

	$N\alpha^{exp}$ (eV)	$N\beta^{exp}$ (eV)	$N\alpha^{MF}$ (eV)	$N\beta^{MF}$ (eV)	$N\beta^{WS}$ (eV)	η_{\uparrow}	η_{\downarrow}
ZnO:Co	—	1.0 (or -0.6) ^a ; -3.4 ^b	0.34	-1.82	-1.36	0.34	-0.36
ZnS:Co	—	—	0.21	-2.64	-2.24	0.03	-0.49
ZnSe:Co	—	-2.2 ^c	0.33	-2.50	-1.98	0.02	-0.31
ZnTe:Co	0.31 ^d	-3.03 ^d	0.28	-2.44	-1.88	0.04	-0.34

^aMagneto optical measurements, Ref. 47.

^bX-ray absorption, Ref. 24.

^cMagneto optical measurements, Ref. 48.

^dMagneto optical measurements, Ref. 49.

states (DOS) of MnZn₃₁O₃₂ (see Fig. 4). A split band appears for $x = 1/32$, but not for $x = 1/4$. The split band indicates localization of the hole state, whereas its merging with the valence band for $x = 1/4$ corresponds to a localization-delocalization transition with increasing doping. (The accurate description of this transition requires however a better treatment of disorder and correlation effects.) The Mn 3d majority spin states (upper part

of the Figure) are strongly hybridized with the valence band. Its center of gravity is located at about 3.5 eV below the top of the valence band. The minority Mn 3*d* states (lower part) on the contrary, are barely visible on the Figure; they start to appear at 6 eV. The split band is of mainly O character with a high Mn contribution. A more close analysis indicates that it is mainly localized on the 2*p* orbitals of the nearest O neighbors of the Mn impurity. As it is visible in the Figure, due to the isovalent impurity, the Fermi level is located just above the split band. Holes may be created by doping (either chemically or in the photoemission process). A partially filled split band corresponds to an uncompensated oxygen down spin which turns around the localized Mn up spin. That picture has a great analogy to the Zhang-Rice singlet (ZRS) state⁵⁰ in cuprates. In cuprates the ZRS can qualitatively be described by the LSDA+*U* method in a similar manner than here.

A localized hole state leads to several consequences. First of all, it prevents ferromagnetism if the doped holes are all trapped in localized states. Second, the exciton seen in magneto-optics is built with holes at the valence band edge and cannot be built with localized holes. However, as it is visible in Fig. 4, the valence band edge is split in the opposite direction (apparent ferromagnetic coupling) and to a much smaller amount (about 1/3 of ΔE^v). Therefore, strictly speaking, magneto-optics does not measure $N\beta$ but an apparent $N\beta^{app}$ of the opposite sign and of smaller amplitude. Our LSDA+*U* calculation for ZnO:Mn explains this discrepancy between $N\beta^{app}$ measured in magneto-optics and the pure antiferromagnetic $N\beta$ parameter (see Table III). Experimentally, the ferromagnetic sign of $N\beta^{app}$ was recently unambiguously demonstrated for GaN:Fe which is not a II-VI SC, however.²¹ The difference between $N\beta$ and $N\beta^{app}$ can also be calculated in the Wigner-Seitz or in other approaches.²⁰

In contrast to ZnO:Mn we find no localization in ZnO:Co, but a situation quite close to it. In the corresponding DOS (not shown) the split band has merged with the valence band. It was already noted that in the LSDA calculations all 3*d* states are much higher in energy than in the LSDA+*U* (which contradicts however the photoemission measurements and is an artefact of LSDA). Therefore, we find hole localization in LSDA for all compounds besides ZnTe. Correspondingly, the $|N\beta|$ values are much higher ($N\beta^{MF} = -3.90, -2.80, -2.43,$ and -2.00 eV for ZnA:Mn with A=O, S, Se, and Te; and $N\beta^{MF} = -3.86, -4.72, -4.30,$ and -4.25 eV for ZnA:Co). That contradicts the experimental data already in the weak coupling compounds ZnSe:Mn and ZnTe:Mn. The relevance of the LSDA+*U* approach to calculate

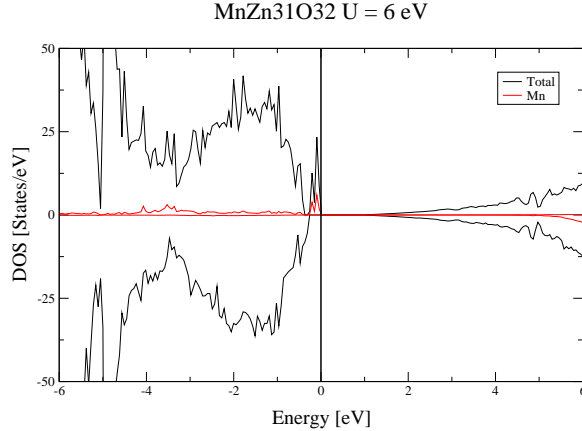


FIG. 4: (Color online) LSDA+ U density of states for $\text{MnZn}_{31}\text{O}_{32}$ ($U = 6$ eV, black: total DOS, red: partial Mn-DOS).

$N\beta$ for ZnSe:Mn was first noted in Ref. 51 which is in excellent agreement with our results. On the other hand, the $N\alpha$ values, are not very much changed by the U parameter.

VI. DISCUSSION

Before comparing our results with other work let us mention the limitations of our procedure. After all, the LSDA+ U treats correlation effects only in an approximative manner and neglects fluctuations. This might explain the discrepancy for ZnO:Co where state localization is very probable in view of the large difference between photoemission and magneto-optics.^{20,21} A more sophisticated method to treat correlation effects will probably refine the picture presented here. It means that the LSDA+ U approach underestimates the localization tendency (and probably also the $|N\beta|$ values) in the strong coupling case. Other error sources are the limited knowledge on U , the use of the effective mass approximation in the Wigner-Seitz approach, which is furthermore restricted to only one valence band in difference to the real band structure.

Our results show good agreement between theory and experiment for J_{dd} , $N\alpha$ and for $N\beta$ in the weak coupling regime (principally ZnTe and ZnSe). However, in the strong coupling case, we would like to argue that our calculated $N\beta$ values correspond neither to the published ones from magneto-optics (see discussion above) nor to those from photoemission. Since the photoemission values of -2.7 (-3.4 eV) for ZnO:Mn (ZnO:Co) were obtained in an

TABLE V: Photoemission data for Hubbard correlation U_{eff} , charge transfer energy Δ_{eff} , and hybridization parameter t_{pd} , as well as the determined $N\beta$ values according to Ref. 22. The p - d and the nearest-neighbor d - d exchange J_{dd} are determined according to the perturbation formulas of Larson *et al*, Ref. 52.

	Δ_{eff} (eV)	U_{eff} (eV)	t_{pd} (eV)	$N\beta$ (eV)	J_{dd} (meV)
ZnO:Mn	7.71	9.61	0.80	-2.7	-25.29
ZnS:Mn	4.21	8.41	0.65	-1.3	-1.29
ZnSe:Mn	3.21	8.41	0.56	-1.0	-0.39
ZnTe:Mn	2.71	8.41	0.51	-0.9	-0.21

indirect way using the perturbation formula of Larson *et al*:⁵²

$$N\beta = -\frac{16}{S}t_{pd}^2 \left[\frac{1}{U_{eff} - \Delta_{eff}} + \frac{1}{\Delta_{eff}} \right]. \quad (11)$$

The experimental core-level photoemission spectra²² were fitted by the configuration interaction (CI) method to a MnA_4 cluster (with the anions $A=O, S, Se,$ and Te) which fixes the hybridization parameter t_{pd} , the Hubbard correlation in the d shell U_{eff} and the effective charge transfer energy between p - and d -orbitals Δ_{eff} (for more details see Ref. 22). The obtained parameters are repeated in Table V and allow to determine $N\beta$ according to Eqn. (11). The $N\beta$ value of -3.4 eV for ZnO:Co was obtained by an identical procedure.²⁴ In the same perturbation approach we may, however, also calculate the nearest-neighbor exchange:⁵²

$$J_{dd} = -\frac{8.8}{2S^2}t_{pd}^4 \left[\frac{1}{U_{eff}(U_{eff} - \Delta_{eff})^2} - \frac{1}{(\Delta_{eff} - U_{eff})^3} \right]. \quad (12)$$

The calculated values are also given in Table V and show large discrepancies to the experimental results (see Table I above) especially in the strong coupling case of ZnO:Mn. Similar discrepancies can be observed by determining the hybridization parameter $t_{pd} = (pd\sigma)/3 - 2\sqrt{3}(pd\pi)/9$ by band structure calculations.⁵³ These difficulties prove that the perturbation formulas (11,12) have a restricted applicability and have to be treated with care especially for strong coupling.

Being close in spirit to Ref. 20, our results deviate nevertheless quite considerably in the numerical values for $N\beta$ which were assumed there. We found a much smaller coupling and we believe that the discrepancy with the published photoemission (PE) values (which are

about two times larger than our results) results from the non-justified use of the perturbative Larson formula in analyzing the PE data. As a consequence, our magnitude of the dimensionless coupling parameter $\eta_{\downarrow} = -1.12$ for ZnO:Mn is much smaller than that estimated in Ref. 20 (between -2.0 and -3.3). It is highly probable, that the reduced value of $|N\beta|$ will also reduce the proposed ferromagnetic Curie temperature in ZnO:Co and ZnO:Mn provided that the doping level is sufficiently high to delocalize the hole states.

The large discrepancies between different experimental and theoretical approaches for $N\beta$ in the strong coupling regime point also to the limitations of the oversimplified model Hamiltonian (3) in that limit. The p - d hybridization t_{pd} can then no longer be regarded as a perturbation and the approximation of an infinite valence band width will probably lead to wrong conclusions. It is highly questionable that the strong coupling case can still be analyzed in such a manner.

We thank Anatole Stepanov, Sergei Ryabchenko, and Roman Kuzian for useful discussions. Financial support from the "Dnipro" (14182XB) program is gratefully acknowledged.

-
- ¹ F. Matsukura, H. Ohno, A. Shen, and Y. Sugawara, Phys. Rev. B **57**, R2037 (1998).
² K. Olejnik, M.H.S. Owen, V. Novák, J. Mašek, A.C. Irvine, J. Wunderlich, and T. Jungwirth, Phys. Rev. B **78**, 054403 (2008).
³ R.W. Cochrane, M. Plischke, and J.O. Ström-Olsen, Phys. Rev. B **9**, 3013 (1974).
⁴ T. Story, R.R. Galazka, R.B. Frankel, and P.A. Wolff, Phys. Rev. Lett. **56**, 777 (1986).
⁵ D. Ferrand, J. Cibert, A. Wasiela, C. Bourgoignon, S. Tatarenko, G. Fishman, T. Andrearczyk, J. Jaroszyński, S. Koleśnik, T. Dietl, B. Barbara, and D. Dufeu, Phys. Rev. B **63**, 085201 (2001).
⁶ G. Schmidt, D. Ferrand, L.W. Molenkamp, A.T. Filip, and B.J. van Wees, Phys. Rev. B **62**, R4790 (2000).
⁷ C. Zener, Phys. Rev. **81**, 440 (1950); **83**, 299 (1950).
⁸ T. Dietl, H. Ohno, and F. Matsukura, Phys. Rev. B **63**, 195205 (2001).
⁹ H.J. Lee, S.-Y. Jeong, C. R. Cho and C. H. Park, Appl. Phys. Lett. **81**, 4020 (2002).
¹⁰ W. Prellier, A. Fouchet, B. Mercey, C. Simon and B. Raveau, Appl. Phys. Lett. **82**, 3490 (2003).
¹¹ P. Sharma, A. Gupta, K.V. Rao, F.J. Owens, R. Sharma, R. Ahuja, J.M.O. Guillen, B. Johans-

- son, and G.A. Gehring, *Nat. Mater.* **2**, 673 (2003).
- ¹² G. Lawes, A. S. Risbud, A. P. Ramirez and R. Seshadri, *Phys. Rev. B* **71**, 045201 (2005).
- ¹³ P. Sati, R. Hayn, R. Kuzian, S. Regnier, S. Schäfer, A. Stepanov, C. Morhain, C. Deparis, M. Läugt, M. Goiran and Z. Golacki, *Phys. Rev. Lett.* **96**, 017203 (2006).
- ¹⁴ S.W. Yoon, S.-B. Cho, S.C. We, S. Yoon, B.W. Suh, H.K. Song, and Y.J. Shin, *Journal of Applied Physics* **93**, 7879 (2003).
- ¹⁵ T. Dietl, T. Andrearczyk, A. Lipińska, M. Kiecana, M. Tay, and Y. Wu, *Phys. Rev. B* **76**, 155312 (2007).
- ¹⁶ K. Sato and H. Katayama-Yoshida, *Physica E* **10**, 251 (2001).
- ¹⁷ T. Chanier, M. Sargolzaei, I. Opahle, R. Hayn, and K. Koepernik, *Phys. Rev. B* **73**, 134418 (2006).
- ¹⁸ *Diluted Magnetic Semiconductors*, edited by J.K. Fordyna and J. Kossut, *Semiconductors and Semimetals Vol. 25* (Academic Press, New York, 1988).
- ¹⁹ C. Benoit á la Guillaume, D. Scalbert, and T. Dietl, *Phys. Rev. B* **46**, 9853 (1992).
- ²⁰ T. Dietl, *Phys. Rev. B* **77**, 085208 (2008).
- ²¹ W. Pacuski, P. Kossacki, D. Ferrand, A. Golnik, J. Cibert, M. Wegscheider, A. Navarro-Quezada, A. Bonanni, M. Kiecana, M. Sawicki, and T. Dietl, *Phys. Rev. Lett.* **100**, 037204 (2008).
- ²² T. Mizokawa, T. Nambu, A. Fujimori, T. Fukumura, and M. Kawasaki, *Phys. Rev. B* **65**, 085209 (2002).
- ²³ J. Okabayashi, K. Ono, M. Mizuguchi, M. Oshima, S.S. Gupta, D.D. Sarma, T. Mizokawa, A. Fujimori, M. Yuri, C.T. Chen *et al.*, *J. Appl. Phys.* **95**, 3573 (2004).
- ²⁴ J. Blinowski, P. Kacman, and T. Dietl, *Spintronics*, MRS Symposia Proceedings No. 690 (Materials Research Society, Pittsburgh, 2002), p. F6.
- ²⁵ J.C. Jamieson and H.H. Demarest, *J. Phys. Chem. Solids* **41**, 963 (1980).
- ²⁶ *CRC Handbook of Chemistry and Physics*, 70th ed., edited by R.C. Weast, D.R. Lide, M.J. Astle and W.H. Beyer, (Chemical Rubber, Boca Raton, 1990), pp. E-106 and E-110.
- ²⁷ T.M. Sabine and S. Hogg, *Acta Cryst. B* **25**, 2254 (1969).
- ²⁸ K. Koepernik and H. Eschrig, *Phys. Rev. B* **59**, 1743 (1999).
- ²⁹ J.P. Perdew and Y. Wang, *Phys. Rev. B* **45**, 13244 (1992).
- ³⁰ V.I. Anisimov, J. Zaanen, and O.K. Andersen, *Phys. Rev. B* **44**, 943 (1991).

- ³¹ H. Eschrig, K. Koepernik, and I. Chaplygin, *J. Solid State Chem.* **176**, 482 (2003).
- ³² O. Gunnarsson, A.V. Postnikov, and O.K. Andersen, *Phys. Rev. B* **40**, 10407 (1989).
- ³³ X. Gratens, V. Bindilatti, N.F. Oliveira Jr., Y. Shapira, S. Foner, Z. Golacki, and T.E. Haas, *Phys. Rev. B* **69**, 125209 (2004).
- ³⁴ Y. Shapira and V. Bindilatti, *Journal of Applied Physics* **92**, 8 (2002).
- ³⁵ T.M. Giebultowicz, J.J. Rhyne, and J.K. Furdyna, *Journal of Applied Physics* **61**, 3587 (1987).
- ³⁶ S. Foner, Y. Shapira, D. Heiman, P. Becla, R. Kershaw, K. Dwight, and A. Wold, *Phys. Rev. B* **39**, 11793 (1989).
- ³⁷ J.P. Lascaray, A. Bruno, M. Nawrocki, J.M. Broto, J.C. Ousset, S. Askenazy, and R. Triboulet, *Phys. Rev. B* **35**, 6860 (1987).
- ³⁸ L.M. Corliss, J.M. Hastings, S.M. Shapiro, Y. Shapira, and P. Becla, *Phys. Rev. B* **33**, 608 (1986).
- ³⁹ A. Stepanov, private communication (2007).
- ⁴⁰ T.M. Giebultowicz, P. Klosowski, J.J. Rhyne, T.J. Udovic, J.K. Furdyna, and W. Girit, *Phys. Rev. B* **41**, 504 (1990).
- ⁴¹ T.M. Giebultowicz, J.J. Rhyne, J.K. Furdyna, and P. Klosowski, *Journal of Applied Physics* **67**, 5096 (1990).
- ⁴² S.M. Ryabchenko, Yu. G. Semenov, and O.V. Terletsii, *Phys. Stat. Sol. (b)* **144**, 661 (1987).
- ⁴³ S. Sanvito, P. Ordejon, and N.A. Hill, *Phys. Rev. B* **63**, 165206 (2001).
- ⁴⁴ W. Przewdzicka, E. Kaminska, M. Kiecana, M. Sawicki, L. Klopotoski, W. Pacuski, and J. Kossut, *Solid State Commun.* **139**, 541 (2006).
- ⁴⁵ A. Twardowski, T. Dietl, and M. Demianiuk, *Solid State Commun.* **48**, 845 (1983).
- ⁴⁶ D. Heimann, Y. Shapira, and S. Foner, *Solid State Commun.* **51**, 603 (1984).
- ⁴⁷ W. Pacuski, D. Ferrand, J. Cibert, C. Deparis, J.A. Gaj, P. Kossacki, and C. Morhain, *Phys. Rev. B* **73**, 035214 (2006).
- ⁴⁸ A. Twardowski, H.J.M. Swagten, and W.J.M. de Jonge, *II-VI Semiconductor Compounds*, edited by M. Jain (World Scientific, Singapore, 1993), p. 227v and Ref. therein.
- ⁴⁹ M. Zielinski, C. Rigaux, A. Lemaitre, A. Mycielski, and J. Deportes, *Phys. Rev. B* **53**, 674 (1996).
- ⁵⁰ F.C. Zhang and T.M. Rice, *Phys. Rev. B* **37**, 3759 (1988).
- ⁵¹ L.M. Sandratskii, *Phys. Rev. B* **68**, 224432 (2003).

⁵² B.E. Larson, K.C. Hass, H. Ehrenreich, and A.E. Carlsson, Phys. Rev. B **37**, 4137 (1988).

⁵³ T. Chanier, Thèse de Docteur, Université de Provence, Marseille (2008)
(<http://tel.archives-ouvertes.fr>, No.: tel-00363983).